Equilibrium and metastable phase transitions in silicon nitride at high pressure: A first-principles and experimental study

Bin Xu,[1,2,*] Jianjun Dong,[1] Paul F. McMillan,[3,4] Olga Shebanova,[3,5] and Ashkan Salamat[3,6]

[1]*Physics Department, Auburn University, Auburn, Alabama 36849, USA*

[2]*Département de Physique, Université de Liège, allée du 6 Août 17, B-4000 Sart Tilman, Belgium*

[3]*Department of Chemistry and Materials Chemistry Centre, Christopher Ingold Laboratories, University College London, 20 Gordon Street, London WC1H 0AJ, United Kingdom*

[4]*Davy-Faraday Research Laboratory, Royal Institution of Great Britain, 21 Albemarle Street, London W1X 4BS, United Kingdom*

[5]*HPCAT, Advanced Photon Source, Argonne, USA*

[6]*The European Synchrotron Radiation Facility (ESRF), Grenoble, France*

(Received 12 November 2010; revised manuscript received 10 April 2011; published 27 July 2011)

We have combined first-principles calculations and high-pressure experiments to study pressure-induced phase transitions in silicon nitride (Si_3N_4). Within the quasi-harmonic approximation, we predict that the α phase is always metastable relative to the β phase over a wide pressure-temperature range. Our lattice vibration calculations indicate that there are two significant and competing phonon-softening mechanisms in the β-Si_3N_4, while phonon softening in the α-Si_3N_4 is rather moderate. When the previously observed equilibrium high-pressure *and* high-temperature $\beta \rightarrow \gamma$ transition is bypassed at room temperature (RT) due to kinetic reasons, the β phase is predicted to undergo a first-order structural transformation to a denser $P\bar{6}$ phase above 39 GPa. The estimated enthalpy barrier height is less than 70 meV/atom, which suggests that the transition is kinetically possible around RT. This predicted new high-pressure metastable phase should be classified as a "postphenacite" phase. Our high-pressure x-ray diffraction experiment confirms this predicted RT phase transition around 34 GPa. No similar RT phase transition is predicted for α-Si_3N_4. Furthermore, we discuss the differences in the pressure dependencies of phonon modes among the α, β, and γ phases and the consequences on their thermal properties. We attribute the phonon modes with negative Grüneisen ratios in the α and β phases as the cause of the predicted negative thermal expansion coefficients (TECs) at low temperatures in these two phases, and predict no negative TECs in the γ phase.

DOI: 10.1103/PhysRevB.84.014113 PACS number(s): 61.50.Ks, 63.20.−e, 63.70.+h, 65.40.−b

I. INTRODUCTION

Silicon nitride (Si_3N_4) is known to have excellent mechanical strength, high thermal stability, and low mass density. Its mechanical and thermal properties at ambient pressure have been investigated extensively by both experiment and theory,[1,2] due to its wide applications as cutting tools, antifriction bearings,[1] and etch masks in microelectronics.[2] In contrast, its properties at high pressure (HP) are less known. Prior to the discovery of the cubic spinel-structured γ-Si_3N_4 (or c-Si_3N_4, $Fd\bar{3}m$) phase at HP and high temperature (HT),[3–7] the structurally related hexagonal α ($P3_1c$) and β ($P6_3/m$) phases were the only two bulk crystalline polymorphs of Si_3N_4 known to exist. Both α and β phases can be synthesized by nitriding pure silicon.[8,9]

The relative phase stability between α and β phases has been a topic of investigation for many years. Direct measurements of energetics of Si_3N_4 were reported by Liang *et al.*[10] However, the difference in formation enthalpies between α- and β-Si_3N_4 was found to be less than the intrinsic experimental uncertainty of ±22 kJ/mol (±32.6 meV/atom). Nevertheless, the β phase is believed to be the ground state of Si_3N_4 because no $\beta \rightarrow \alpha$ transition was ever observed. The stability condition for the α phase has been experimentally studied at temperatures of 1300°−1800 °C and pressures up to 60 GPa.[11–18] Pure single-crystal α-Si_3N_4 shows no sign of transformation at temperatures up to 1820°−2200 °C.[18,19] However, the $\alpha \rightarrow \beta$ transformation is observed to occur at ambient pressure and HTs in the presence of Y_2O_3 or other oxides. From the observed liquid phases on the α-Si_3N_4 surfaces, Suematsu *et al.* proposed a solution-precipitation mechanism for the $\alpha \rightarrow \beta$ transformation.[18] They claimed that first the catalyst oxides form a liquid phase with Si_3N_4 on the surface at HTs. Then, through atomic transportation in the liquid, small particles of β-Si_3N_4 emerge. The liquid phase on the α-Si_3N_4 surfaces is believed to play an important role to lower the activation energy of atomic transportation. The stability of pristine α-Si_3N_4 at HTs is ascribed to the extremely high value of the activation energy with clean surfaces. On the theory side, several studies confirmed that the static binding energy of an α phase is slightly higher than that of a β phase.[8,20–22] Wendel and Goddard[21] and Kuwabara *et al.*[22] carried out calculations using a statistical quasi-harmonic approximation (QHA), and they both found that the α phase remains metastable in the temperature range from 0 to 2000 K at ambient pressure. Yet, pressure effects on the relative thermodynamic stability between α and β phases was not addressed in previous theoretical studies.

Pressure-induced structural phase transitions in Si_3N_4 have drawn extensive attention since 1999. Experiments showed that the cubic spinel γ-Si_3N_4 can be obtained from both hexagonal α- and β-Si_3N_4 upon compression and simultaneous *in situ* heating.[3–7] The γ phase is quenchable to the ambient condition, and it remains stable at temperatures ranging up to about 1670 K at ambient pressure.[23,24] When γ-Si_3N_4 "decomposes"

at ambient pressure upon heating, the samples may consist of both α- and β-Si_3N_4.[23] Previous *ab initio* studies have calculated the $\beta \rightarrow \gamma$ transition pressure (P_t) at adiabatic static condition,[3,25] as well as at HTs.[22,26] The predicted equilibrium transition pressure P_t increases only slightly with the increase of temperature. Several hypothetical postspinel HP phases have also been proposed by first-principles calculations.[27,28] For example, a $CaTi_2O_4$-type postspinel phase is predicted to be thermodynamically more stable than the spinel γ phase at pressures higher than 160 GPa. Yet, none of the predicted new phases has been confirmed experimentally.

The *in situ* heating to HT is found to be critical for synthesizing the γ-Si_3N_4 at HPs. At room temperature (RT), the $\beta \rightarrow \gamma$ transition is, however, bypassed. Zerr found that β-Si_3N_4 exists up to 34 GPa and it then transforms into an unknown phase (labeled the δ phase) under further compression.[29] The new $\gamma \rightarrow \delta$ phase transition was observed by both Raman spectroscopy and energy-dispersive x-ray powder diffraction (EDXD) measurements. But the structure of the δ phase was not fully determined. Zerr proposed three possible unit cells based on the measured EDXD pattern: two tetragonal and one orthorhombic. The first hypothetical tetragonal unit cell has a density of 4.05 g/cm^3 at 42.6 GPa, which is smaller than that of γ-Si_3N_4 (4.50 g/cm^3). At the same pressure, the second tetragonal and the orthorhombic structures were proposed to have densities of 4.56 g/cm^3 and 5.16 g/cm^3, respectively, which are both larger than that of the γ phase. The latter two structures are considered as "postspinel" phases. Zerr further suggested that the δ-Si_3N_4 should be considered as a metastable intermediate stage in the $\beta \rightarrow \gamma$ transition. Kroll proposed a metastable willemite-II-Si_3N_4 phase as an intermediate between β- and γ-Si_3N_4 in both energetics and density.[25] However, the willemite-II (wII) phase is unlikely to be the experimentally observed δ phase because 1) the wII phase, which is structurally closely related to the spinel γ-Si_3N_4, has been shown to have a significantly lower activation barrier for the $\gamma \rightarrow$ wII transformation, comparing to that of $\gamma \rightarrow \beta$ transformation.[25] Although the activation barrier of the $\beta \rightarrow$ wII transformation is unknown, it is more likely to be high enough to exclude the RT transition. And 2) the calculated Raman frequencies of wII-Si_3N_4 could not match many strong peaks appearing in the measurements,[29,30] e.g., two observed peaks at about 500 and 550 cm^{-1} at 38.2 GPa are absent for the wII phase.

Meanwhile, β-Ge_3N_4, which is isostructural to β-Si_3N_4, is found to transform into the metastable polymorph δ-Ge_3N_4 with hexagonal $P3$ symmetry at RT.[31] An *ab initio* calculation from Dong *et al.* showed that a $\beta \rightarrow P\bar{6} \rightarrow P3$ transition sequence could occur in Ge_3N_4 at pressures of about 20 and 28 GPa, respectively,[32] which are of second order driven by soft phonons. If β-Ge_3N_4 directly transforms into the $P3$ structure, the transition was predicted to be first order and $P_t =$ ~23 GPa. Dong *et al.* also pointed out that the $\beta \rightarrow P\bar{6}$ transition originated from a soft silent B_u mode. From the experimental side, McMillan *et al.* published the Raman studies,[33] and Soignard *et al.* carried out the x-ray work.[31] These RT experiments confirmed the direct $\beta \rightarrow P3$ transition which is associated with a 5%–7% volume reduction. The Raman data they observed exclude the intermediate $P\bar{6}$ structure. Based on density considerations, Soignard *et al.* suggested that the new polymorph is a "postphenacite" phase, in stead of "postspinel." Comparison of the x-ray diffraction and Raman data between Ge_3N_4 and Si_3N_4 shows similarities which may suggest a $P3$ or related structure for δ-Si_3N_4. It is still unclear whether there are intrinsic differences between the HP-RT behaviors of Si_3N_4 and Ge_3N_4, or the experimental results may be interpreted differently.

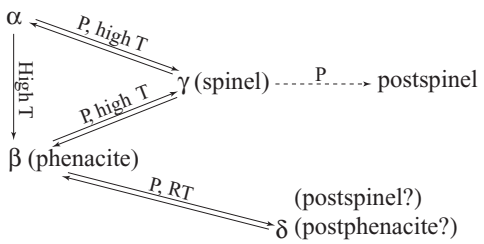

FIG. 1. Polymorphs of Si_3N_4 and synthesis conditions.

In this paper, we present a series of systematic first-principles studies for thermodynamic properties of Si_3N_4 polymorphs over a wide pressure-temperature range based on the statistical QHA. The current knowledge of pressure-temperature (P-T) conditions for various experimentally confirmed and theoretically hypothesized polymorphs is sketched in Fig. 1. In our study, the three main focuses are these: 1) What is the HP and HT equilibrium solid phase diagram in Si_3N_4? Is the α phase always a metastable phase relative to the β phase in Si_3N_4? What is the phase boundary between the β and γ phases? 2) Does the HP δ phase have a "postphenacite" or "postspinel" structure? Which role does the vibrational instability (i.e. softening phonons) play in the RT $\beta \rightarrow \delta$ phase transitions? 3) How do the vibrational instabilities affect equilibrium thermal properties in the two hexagonal phases of Si_3N_4? Does the cubic spinel-structured Si_3N_4 have any negative thermal expansion at low temperatures?

The rest of this paper is organized as follows. In Sec. II, we introduce the methods of our calculations and experiments. In Sec. III, we compare the thermodynamic stability among the three known phases (α, β, and γ) using the first-principles-calculated thermodynamic potentials, and predict the equilibrium T-P phase transition conditions. Next, we investigate the structural instabilities and possible metastable phase transitions from both theory and experiment for β-Si_3N_4 at HPs and RT. The stability of the α phase under HP is also discussed on theoretical grounds. Then, we further obtain the measurable thermal properties of Si_3N_4, such as the thermal expansion coefficient (TEC), heat capacity and bulk Grüneisen parameter at zero pressure and HPs. Our zero-pressure results are compared with available experimental data[34–41] and previous calculations.[21,22,42,43] Conclusions are drawn in Sec. IV.

II. COMPUTATIONAL AND EXPERIMENTAL METHODS

A. First-principles calculation

In this paper, the equilibrium T-P phase diagrams and thermodynamic properties are predicted using first-principles-calculated thermodynamic potentials. As an insulator, the

Helmholtz free energy of a bulk crystalline Si_3N_4 system consists of two parts:

$$F(T,V) = E_{\text{static}}(V) + F_{\text{vib}}(T,V), \tag{1}$$

where $E_{\text{static}}(V)$ is the static binding energy of the system and $F_{\text{vib}}(T,V)$ is the vibrational free energy. Free energy associated with the electronic thermal excitation is neglected. $E_{\text{static}}(V)$ for α-, β-, and γ-Si_3N_4 are calculated with unit-cell models of respective crystal symmetries. We adopted the density functional theory (DFT) with a plane-wave basis set and ultrasoft pseudopotentials (US-PPs),[44] which is implemented in the VASP code.[45] The exchange and correlation functional is treated with the local density approximation (LDA). Plane-wave basis functions with energies up to 347.9 eV were used. A total energy change of 10^{-9} eV per unit cell was chosen as the convergence criterion for the self-consistent iterations. The Brillouin zone integration in our total energy calculations was approximated with the Monkhorst–Pack method, with grids of $4 \times 4 \times 6, 4 \times 4 \times 12$, and $6 \times 6 \times 6$ for α-, β-, and γ-Si_3N_4, respectively. The calculated total energies at several chosen volumes were fitted to the third-order Birch-Murnaghan equations of state (BM-EOS)[46,47] by the least-squares fitting algorithm.

The vibrational free energy in Eq. (1) is evaluated within the statistical QHA, which can be expressed as

$$F_{\text{vib}}(T,V) = \int_0^\infty \left[\frac{1}{2}\hbar\omega + k_B T \ln\left(1 - \exp\left(\frac{-\hbar\omega}{k_B T}\right)\right)\right] \times g(\omega)\, d\omega, \tag{2}$$

where ω is the harmonic phonon frequency at a given $\boldsymbol{q}$ point and $g(\omega)$ is the vibrational density of state (VDOS). The calculations of VDOS require the frequencies of phonon modes at arbitrary $\boldsymbol{q}$ points in the reciprocal $\boldsymbol{q}$ space, which are derived based on the real-space finite-displacement method. Simply speaking, a small yet finite displacement is first added to a single atom in the fully relaxed large supercell model. Then, the Hellmann–Feynman (HF) forces on all the atoms are calculated for the displaced structure. Neglecting the fourth- and higher order terms, at the condition that the jth atom in the ℓ'th unit cell is displaced by Δ in the β direction, the α component of the HF force on the ith atom in the ℓth unit cell can be expressed as a Taylor expansion in terms of Δ

$$F_{\alpha,i}(\ell) = -\Phi_{\alpha i,\beta j}(\ell,\ell') \cdot \Delta - \tfrac{1}{2} A_{\alpha i,\beta j,\beta j}(\ell,\ell',\ell') \cdot \Delta^2 - \cdots \tag{3}$$

here $\Phi_{\alpha i,\beta j}(\ell,\ell')$ is the element of the force constant matrix. $A_{\alpha i,\beta j,\beta j}(\ell,\ell',\ell')$ is the third-order anharmonic term, which can be canceled out with two force calculations using positive and negative displacements of equal magnitudes. The full set of real-space force constants is generated by the irreducible one, which is derived from group-theoretical analysis based on crystal symmetry. Only the irreducible force constants are calculated directly. In this study, we adopted 168-atom, 168-atom, and 112-atom supercell models for the α, β, and γ phases, respectively. The sizes of the supercell models are large enough to minimize the finite-size artifacts in the calculated real-space force constant matrices.

Phonon frequencies and eigenvectors are yielded from diagonalization of dynamical matrices $D_{\alpha i,\beta j}(\boldsymbol{q})$, which are obtained from the Fourier transformation of the real-space force constant matrices. In an ionic crystal, lattice vibrations of optic phonon modes induce dipole-dipole interactions, which in turn affect the phonon frequencies around the Γ point ($\boldsymbol{q} = 0$). The interaction causes the so-called LO-TO splitting in optic phonon modes. However, this effect is not taken into account in the supercell calculations. We corrected the LO-TO splitting effects with a simple interplanar force constant method proposed by Kunc and Martin.[48]

Within the QHA, the bulk Grüneisen parameter can be obtained from the weighted average of mode Grüneisen ratios [$\gamma_\xi(\boldsymbol{q}) = -\partial(\ln \omega_\xi(\boldsymbol{q}))/\partial(\ln V)$]:

$$\gamma = \frac{\sum_{k,\xi} \gamma_\xi(\boldsymbol{q})\, c_{v,\xi}(\boldsymbol{q})}{\sum_{k,\xi} c_{v,\xi}(\boldsymbol{q})}, \tag{4}$$

where $c_{v,\xi}(\boldsymbol{q})$ is the mode-specific isochoric heat capacity. The mode Grüneisen parameter can be calculated using the HF theorem.

$$\gamma_\xi(\boldsymbol{q}) = -\frac{V}{2\omega_\xi^2(\boldsymbol{q})} \left\langle \mathbf{e}(\boldsymbol{q},\xi) \left| \frac{\partial \mathbf{D}(\boldsymbol{q})}{\partial \mathbf{V}} \right| \mathbf{e}(\boldsymbol{q},\xi) \right\rangle; \tag{5}$$

here V is the volume, $\boldsymbol{D}(\boldsymbol{q})$ is the dynamical matrix, and $\boldsymbol{e}(\boldsymbol{q},\xi)$ is the eigenvector of the ξth normal mode at reciprocal lattice point $\boldsymbol{q}$. In practice, we evaluate the first-order derivative of $\boldsymbol{D}(\boldsymbol{q})$ with respect to the volume approximately using the finite-difference method. This methodology has been applied successfully to our previous study of type II Si clathrate.[49]

B. High-pressure experiment

Polycrystalline β-Si_3N_4 was obtained from Aldrich (>99.99% purity). Powdered samples were loaded into cylindrical screw-driven or membrane diamond anvil cells for Raman and synchrotron x-ray diffraction studies using 4:1 methanol/ethanol or N_2 as pressure-transmitting media. We used preindented Re gaskets with 200–300 holes drilled by electroerosion. Pressure was measured by the ruby fluorescence method.[50] Raman spectra were obtained at University College London using a home-built system.[51] Early x-ray diffraction experiments were carried out at beamline 9.1 at Daresbury SRS (Synchrotron Radiation Source).[52] Later studies were completed at Diamond I15 using $\lambda = 0.444$ Å radiation. The two-dimensional diffraction data were analyzed and transformed to one-dimensional diffraction patterns using Fit2D.[53] Unit-cell parameters and atomic positions were refined by Rietveld and LeBail techniques using Powdercell and GSAS (General Structure Analysis System).[54,55]

III. RESULTS AND DISCUSSION

In this section, we present results from first-principles calculations and HP experiments that were independently conducted. According to our computational methodologies, the static total energies and vibrational frequencies are required to obtain the thermodynamic potentials at finite temperature. The full phonon spectra can also reveal the structural instabilities at desired conditions (e.g., HP). In the following, we will first present our results on the relative stabilities of the three know phases at varied pressures and temperatures, while the

emphasis of our study is the pressure-induced metastable phase transition at room temperature.

A. Crystal structures, static binding energies, and vibrational spectra

Atomic structures of α-, β-, and γ-Si_3N_4 are shown in Fig. 2. Both α- and β-Si_3N_4 have hexagonal symmetry, and they contain similar local bonding: Each Si atom is tetrahedrally bonded to four N atoms (Si-N_4) and each N atom has a threefold trigonal coordinates (N-Si_3). All the SiN_4 tetrahedra are slightly distorted and connected by corner-sharing. The difference between these two phases can be characterized by the stacking sequence along the c axis. The periodicity of α- and β-Si_3N_4 in that direction can be described as ABCDABCD ... and ABAB ... stacking, respectively. From another point of view, α-Si_3N_4 can be interpreted as a complex network formed with nonplanar six-membered (6-atom) rings, whereas β-Si_3N_4 is composed of nonplanar 6-, 8- and 12-membered rings. There are two types of trigonal N-Si_3 units: those with N atoms at the 2a and 2b sites of α-Si_3N_4 or the 2c site of β-Si_3N_4 located at the basal plane perpendicular to the c axis, while the rest of the N-Si_3 units are in the vertical or near-vertical orientations. Most basal N-Si_3 units are perfectly planar with three bonds of equal length and three 120° Si-N-Si bond angles, except that the N-Si_3 units with N at the 2b sites of α-Si_3N_4 form triangular pyramids (i.e., three bonds still have equal length, but the bond angles are less than 120°). The vertical N-Si_3 units are distorted in bond lengths and bond angles which yield distorted pyramidal units. The γ phase has a distinctively different structure, in which Si atoms occupy both tetrahedral (1/3 of Si atoms, 8a sites) and octahedral (2/3 of Si atoms, 16d sites) sites, and all the N atoms are tetrahedrally bonded. This is consistent with the fact that γ-Si_3N_4 is the HP phase which has a larger coordination number. The spinel structure is named after the mineral $MgAl_2O_4$ which has a fcc lattice with space group $Fd\bar{3}m$. For γ-Si_3N_4, there are two formula units in the primitive unit cell and eight units in the conventional cubic cell.

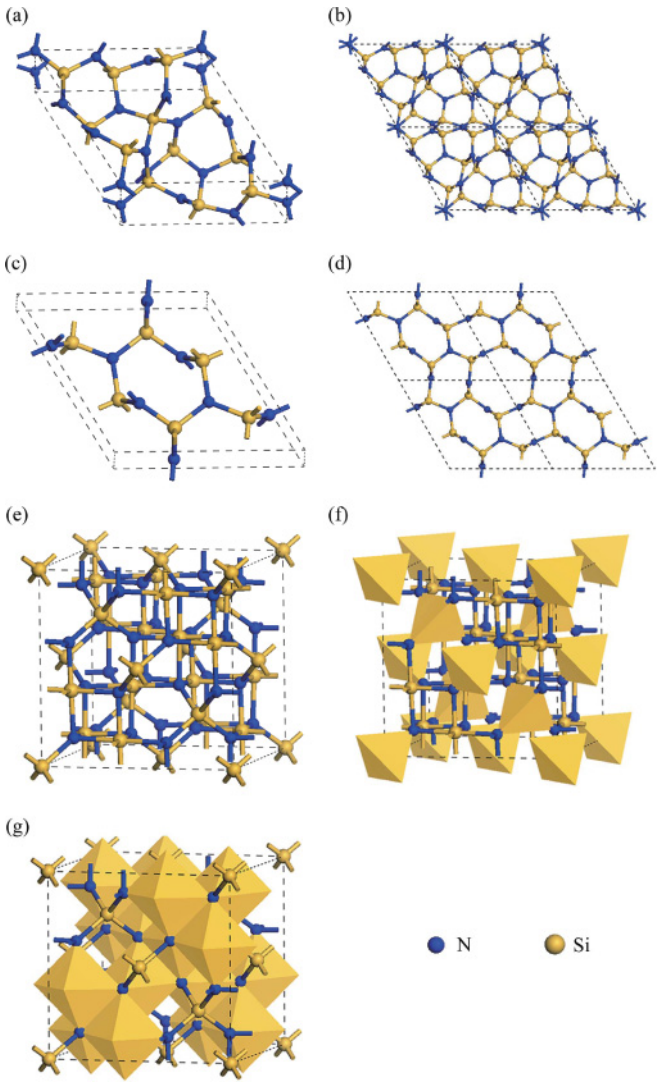

FIG. 2. (Color online) Crystal structures of (a), (b) α-Si_3N_4; (c), (d) β-Si_3N_4; and (e), (f), (g) γ-Si_3N_4. In the panel of α- and β-Si_3N_4, the first graph illustrates the unit-cell model and the second graph is the $2 \times 2 \times 1$ supercell model viewed in the direction of the c axis. In the panel of γ-Si_3N_4, the first graph shows the conventional cubic cell of the spinel structure and the following two graphs show the fourfold and sixfold coordinated Si units (SiN_4 and SiN_6) with tetrahedra and octahedra, respectively.

The calculated E-V data sets of α-, β-, and γ-Si_3N_4 are shown in Fig. 3, and the corresponding fitting parameters from the third-order BM-EOS (E_0, V_0, B and B') are listed in Table I, together with reported experimental[3,6,8,57–59,61–64] and other theoretical results.[20–22,56,60] As the measurements were usually made at RT, our predicted parameters at 300 K within the QHA are also presented. Our calculation has a good overall agreement with other theoretical and experimental results. Compared with the experiments, our calculated static equilibrium volumes are consistently underestimated by about 1%–3%, and the calculated bulk moduli are within the range of reported experimental data, which contain about 5%–15% differences among different reports. The predicted thermal equations of states at 300 K are slightly closer to the measurement. Our results are within the typical accuracy of

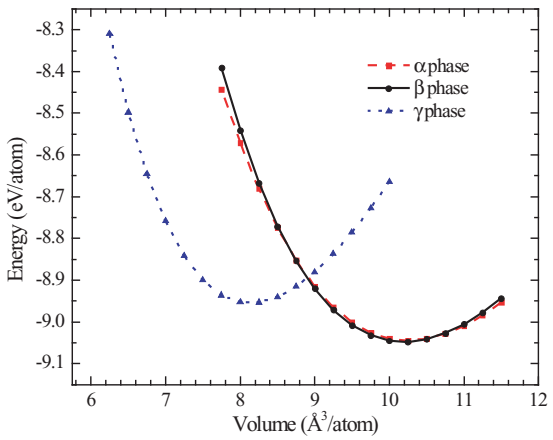

FIG. 3. (Color online) Energy-volume curves for α-, β- and γ-Si_3N_4 in the scale of per atom. The β phase has an equilibrium energy of 3 meV lower than that of the α phase. E_0 of the γ phase is 93 meV higher than the β phase.

TABLE I. Summary of calculated and measured crystal parameters of α-, β-, and γ-Si_3N_4. V_0 is the equilibrium volume per atom, B is the bulk modulus and B' is the first-order pressure derivative.

Si_3N_4	Source	V_0 (Å^3/atom)	B(GPa)	B'
α-Si_3N_4	LDA (this paper, static)	10.260	232	2.583
	LDA (this paper, 300 K)	10.328	226	2.576
	LDA[22]	10.325	240	4.0 (fixed)
	LDA[56]	10.237	257	
	OLCAO[20]	10.542	257	
	Force fields (300 K)[21]	10.806	246	
	Experiment[57]	10.455		
	Experiment[58]	10.445		
	Experiment[59]	10.465	223.4 ($\pm$15)	4.5 ($\pm$1.3)
β-Si_3N_4	LDA (this paper, static)	10.199	241	3.439
	LDA (this paper, 300 K)	10.267	237	3.440
	LDA[22]	10.268	252	4.0 (fixed)
	GGA[60]		237.2–241.5	
	LDA[56]	10.183	225	
	Force fields (300 K)[21]	10.661	266	
	Experiment[61]	10.396		
	Experiment[62]	10.411	270 ($\pm$5)	4.0 ($\pm$1.8)
	Experiment[63]	10.452	232.7	
	Experiment[8]	10.356		
γ-Si_3N_4	LDA (this paper, static)	8.140	308	3.898
	LDA (this paper, 300 K)	8.220	297	3.898
	LDA[22]	8.137	320	4.0 (fixed)
	OLCAO[20]	8.595	280	
	Experiment[64]	8.270	290 ($\pm$5)	4.9 ($\pm$0.6)
	Experiment[6]	8.286	308	4.0
	Experiment[23]	8.261		
	Experiment[63]		300 ($\pm$10)	3.0 ($\pm$0.1)
	Experiment[3]	8.474 ($\pm$0.26)		

OLCAO, orthogonalized linear combination of atomic orbitals; GGA, generalized gradient approximation.

the LDA calculation and they are consistent with the fact that the LDA tends to underestimate the equilibrium volume and overestimate the bulk modulus by a few percent.

Our static total energy calculation shows that the β phase is only slightly energetically more stable (i.e., about 3 meV/atom lower) than the α phase at their respective static equilibrium volumes. Such a small energy difference is consistent with the fact that both α and β phases are found to coexist during different synthesis routes. Also, in agreement with experiment, we find that the calculated β phase has larger density and lower compressibility compared with the α phase. This suggests that the α phase is even less favored thermodynamically at higher pressure relative to the β phase. The relative stability between these two phases will be further examined in later text with the consideration of temperature and pressure effects. For the γ phase, our calculation yields a static equilibrium energy which is 93 meV/atom higher than that of the β phase, and a static equilibrium volume of 2 Å^3/atom smaller than that of the β phase. These results agree with the fact that the spinel-structured γ phase is a HP phase in Si_3N_4.

Figure 4 shows the phonon dispersion curves and VDOS plots of α-, β-, and γ-Si_3N_4 at their respective static equilibrium volumes. All three phases studied here are dynamically stable, i.e., no soft-phonon modes are present. The α and β phases have very similar VDOSs which reflect the similarity in their crystal structures and Si-N bonding. On the other hand, the spinel-structured γ-Si_3N_4 shows some distinctively different characters in its VDOS, comparing with those of α and β phases. HP phases usually have higher vibration frequencies. Yet we find that the top phonon branches in the γ phase have frequencies which are apparently lower than those of α or β phases.

Mode Grüneisen ratios along some high symmetry directions are shown in Fig. 5. Although there are many similarities in the mode Grüneisen ratios between the α and β phases, for example, their low-frequency phonon modes are found to have negative mode Grüneisen parameters while all the HP modes have positive ratios with the upper limit of about 1.5, there are some noticeable differences for phonons around the M-point transverse acoustic (TA) mode and the Γ point optic B_u mode. The phonons close to these two modes in the β phase are found to have large negative Grüneisen ratios, which suggest possible structural instability of the β phase upon compression. On the other hand, the γ-Si_3N_4 shows no negative mode Grüneisen ratios at all, and the values of its mode Grüneisen ratios range from 0.24 to 1.66 at zero pressure.

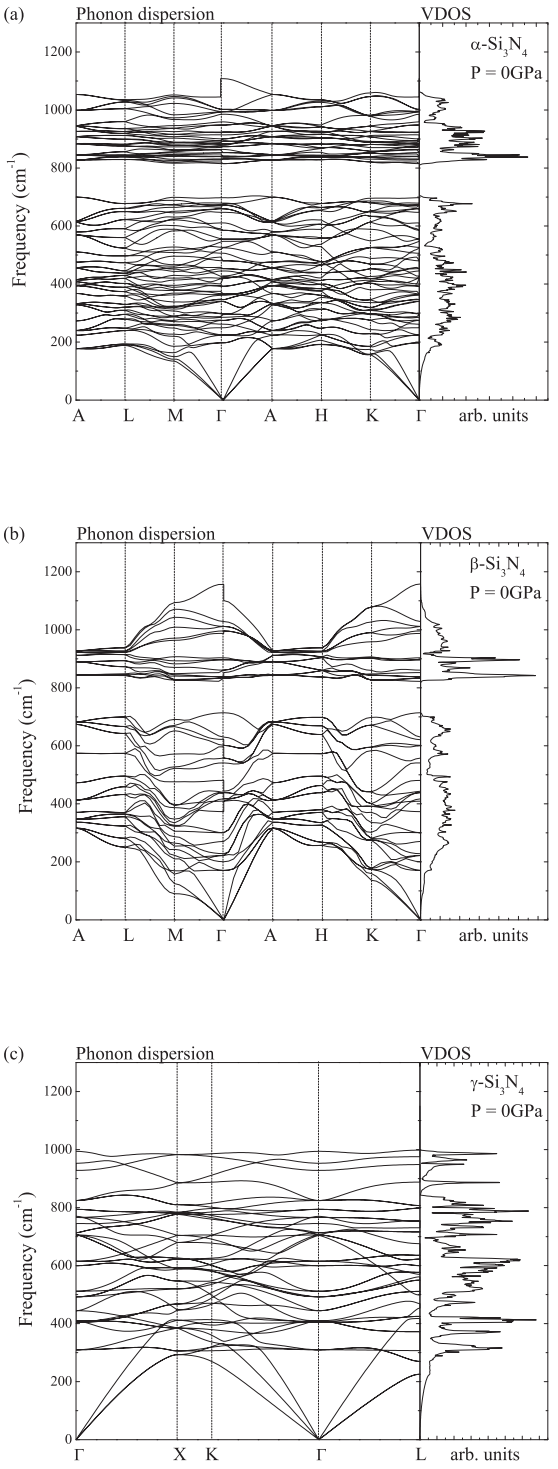

FIG. 4. Phonon dispersion curves and VDOS of (a) α-Si_3N_4; (b) β-Si_3N_4; and (c) γ-Si_3N_4 at zero pressure.

B. Equilibrium thermodynamic stability and phase transitions

To illustrate the relative thermodynamic stability between the α and β phases, we plot the LDA-calculated Gibbs free-energy differences between the two phases at 0, 5, and 10 GPa in Fig. 6. A positive value of $\Delta G_{\alpha-\beta}$ means that α-Si_3N_4 is thermodynamically metastable. At isobaric conditions, the calculated $\Delta G_{\alpha-\beta}$ are almost constant over the temperature range from 0 to 2000 K. At zero pressure, our calculated $\Delta G_{\alpha-\beta}$ is 2.8 meV/atom at 0 K which agrees with Kuwabara's (DFT with PAW+LDA, where PAW is the projector augmented wave) $\Delta F_{\alpha-\beta}$ of 2.6 meV/atom at 0 K. At 2000 K, our $\Delta G_{\alpha-\beta}$ is 2.6 meV/atom, while Kuwabara's $\Delta F_{\alpha-\beta}$ decreases to 1.3 meV/atom. The results of Wendel and Gaddord were based on empirical force field models and they gave an opposite trend of temperature dependence, 0.1 meV/atom at 300 K and 0.7 meV/atom at 2000 K. At elevated pressures, we predict an increasing $\Delta G_{\alpha-\beta}$. At 5 and 10 GPa, $\Delta G_{\alpha-\beta}$ is about 4.6 and 5.9 meV/atom, respectively. We do not predict $\Delta G_{\alpha-\beta}$

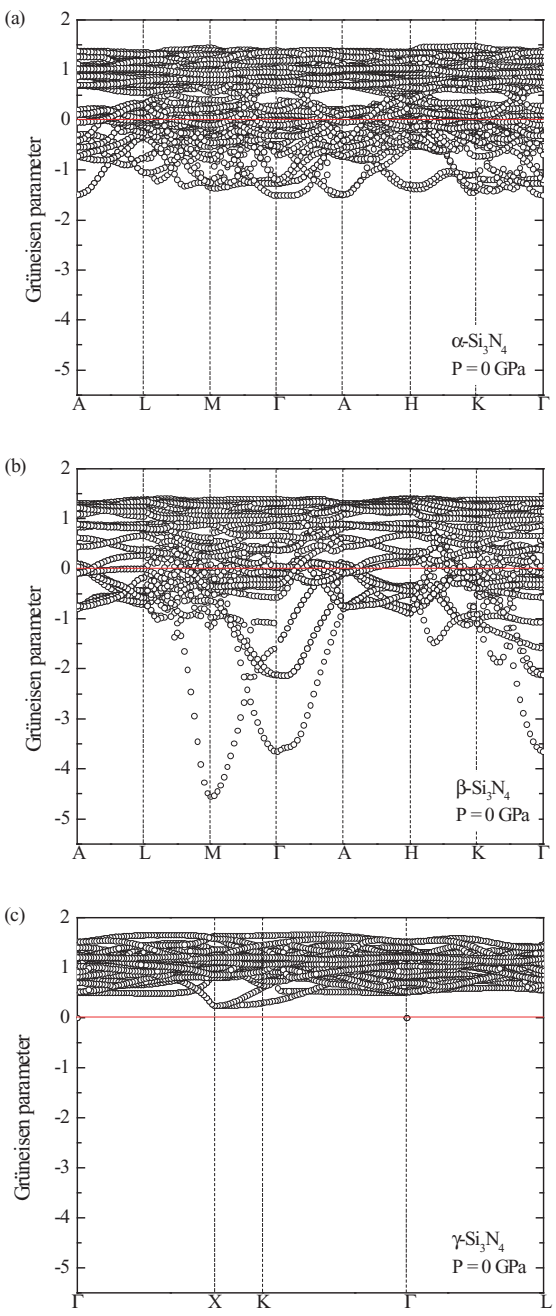

FIG. 5. (Color online) Calculated dispersion curves (scattered circles) of mode Grüneisen parameter of (a) α-Si_3N_4, (b) β-Si_3N_4, and (c) γ-Si_3N_4 at zero pressure. (Red) horizontal line is present to separate the positive and negative values.

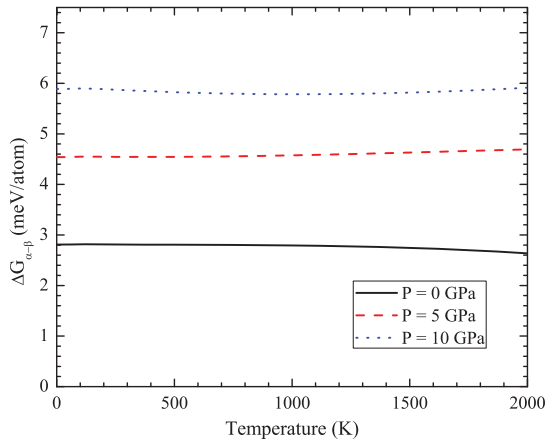

FIG. 6. (Color online) Gibbs free energy of α-Si_3N_4 relative to that of the β phase as a function of temperature. Solid, dashed, and dotted lines represent the pressure of 0, 5, and 10 GPa, respectively.

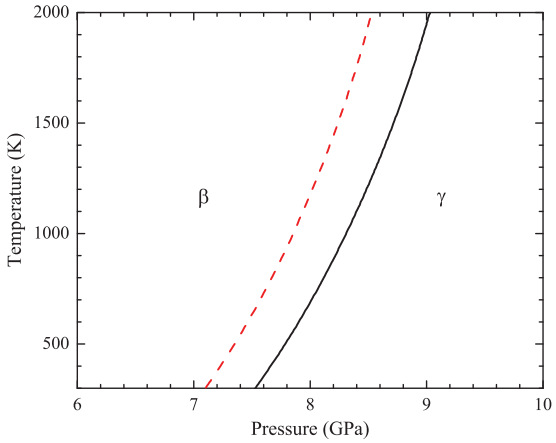

FIG. 7. (Color online) T-P phase diagram of Si_3N_4. Solid curve denotes the phase boundary between β- and γ-Si_3N_4. Dashed curve denotes the phase boundary between α- and γ-Si_3N_4.

at pressures higher than 10 GPa because the β phase starts to show signs of structural instability (see discussion in later text). We conclude that the α phase is metastable compared with the β phase in the temperature range from 0 to 2000 K and at least up to 10 GPa.

Upon compression, both the ground-state β phase and metastable α phase transform into the γ phase. Our predicted equilibrium T-P phase boundaries are shown in Fig. 7. The Clapeyron slopes for the $\beta \rightarrow \gamma$ (solid line) and $\alpha \rightarrow \gamma$ (dashed line) transitions are both positive, which suggests that the HP γ phase has a lower vibrational entropy. Consequently, the transition pressure (P_t) increases with temperature. The predicted P_t of the $\beta \rightarrow \gamma$ transition is 7.5 GPa at 300 K, and it increases to 9.0 GPa at 2000 K. The P_t of the $\alpha \rightarrow \gamma$ transition is about 0.5 GPa lower than that of $\beta \rightarrow \gamma$ transition. Togo and Kroll[26] and Kuwabara *et al.*[22] also predicted a positive Clapeyron slope for the $\beta \rightarrow \gamma$ transition. The small calculated Clapeyron slopes (dP/dT) means that the transitions are primarily volume driven and the equilibrium P_t is not sensitive to the temperature. For example, P_t changes by less than 2 GPa when the temperature rises from 300 to 2000 K. On the experimental side, the transition pressures are scattered from 10 to 36 GPa (Table II). This could be ascribed to the different compositions or impurities of the starting samples being used. Nonetheless, *in situ* heating is required for the synthesis of γ-Si_3N_4 in all experiments. This is a clear indication that large kinetic barriers exist. For better comparison between theory and experiment, we list here only the theoretical results at $T = 2000$ K.

C. Phonon-softening-induced structural instability in β-Si_3N_4 at high pressures

Although β-Si_3N_4 transforms into the γ phase at HPs and HTs, the β phase is stable at the RT up to at least 30 GPa. To investigate the structural stability of the β phase, we calculated the pressure dependence of lattice vibration. First, we examined the phonon modes at the zone center Γ point. Our technique was adopted previously to study the structural and vibrational properties of Ga_2O_3 and Ga_3O_3N.[66,67] For β-Si_3N_4 with space group $P6_3/m$, there are in total 42 vibrational modes. Using group theory, the irreducible representation for Γ-point phonon modes is

$$\Gamma_{\text{acoustic}} = A_u + E_{1u}, \tag{6}$$

$$\Gamma_{\text{optic}} = 4A_g + 2A_u + 3B_g + 4B_u + 2E_{1g} + 5E_{2g} + 4E_{1u} + 2E_{2u}. \tag{7}$$

TABLE II. Summary of phase-transition pressure and temperature for γ-Si_3N_4.

Method	Starting material	P_t (GPa)	Temperature (K)
Experiment			
diamond cell[3]	Si, amorphous Si_3N_4 and polycrystalline $\alpha + \beta$	15	2100
Shock compression[5]	β+2 wt% (Nd_2O_3+Y_2O_3)β	36	1990
Diamond anvil cell[65]	$\alpha + 1\%\beta$	17.5	–
Multianvil[4]	$\alpha + \beta$	17	2100
Shock wave[7]	β	10	2073
Theory			
PAW + GGA[26]	β	13	2000
PAW + LDA[22]	β	6.3	2000
US-PP + LDA (this paper)	α	8.5	2000
US-PP + LDA (this paper)	β	9.0	2000

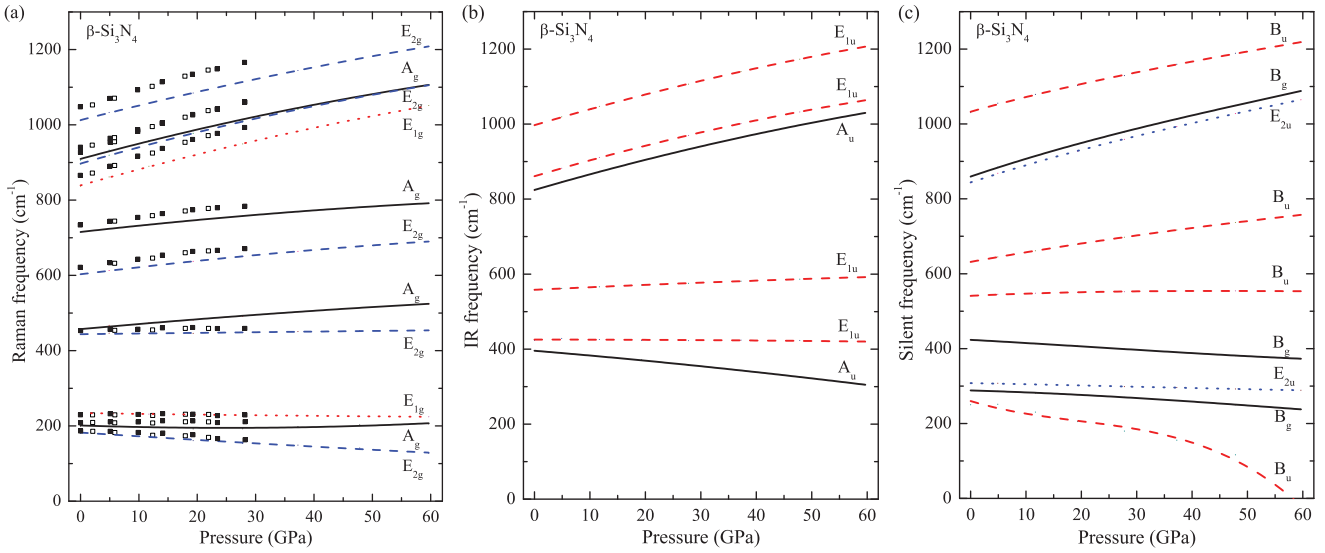

FIG. 8. (Color online) (a) Raman, (b) IR, and (c) silent mode frequencies as a function of pressure up to 60 GPa for β-Si_3N_4. Experimental pressure dependencies of Raman modes up to 30 GPa are also presented in discrete symbols as a comparison.[68] Solid squares denote measurements upon compression and open squares denote measurements upon decompression. Several low-frequency modes are found to decrease with increasing pressure. One B_u branch of the silent modes is found dropping to zero at about 60 GPa.

For the optic modes, 11 modes ($4A_g + 2E_{1g} + 5E_{2g}$) are Raman active, 6 modes ($2A_{2u} + 4E_{1u}$) are infrared (IR) active, and the rest ($3B_g + 4B_u + 2E_{2u}$) are silent modes, among which Raman and IR spectra can be detected in experiments. Figure 8 shows our calculated Raman, IR, and silent modes of the β phase as a function of pressure up to 60 GPa. Experimental pressure dependencies up to 30 GPa are presented for comparison. For the measured Raman modes from Zerr *et al.*,[68] one A_g mode is missing, possibly due to the weak intensity. The rest of the Raman modes match well with our calculation. Our prediction tends to underestimate the frequencies by about 2%–4%, which is typical for calculations of this type. The calculation shows a clear pattern that all low-frequency modes (400 cm^{-1} and below) have zero- or negative-pressure dependencies. The lowest B_u silent mode decreases much faster than the others and eventually vanishes at about 60 GPa. The predicted negative-pressure dependencies in these modes are consistent with the calculated negative mode Grüneisen ratios [Fig. 5(b)]. The calculated Γ-point phonon softening pattern in β-Si_3N_4 is in agreement with our previous results for β-Ge_3N_4.[32]

Next, we extended our study to all the phonon modes in the reciprocal space. Our calculated phonon dispersion curve of β-Si_3N_4 at 48 GPa (Fig. 9) shows that two low-frequency branches decrease dramatically upon compression, i.e., one TA branch along the Γ-M direction and the lowest optic B_u branch. The TA mode goes soft at the Brillouin zone boundary M point, i.e. $\boldsymbol{q} = \frac{2\pi}{a}(\frac{1}{\sqrt{3}},0,0)$, and the optic mode goes soft at the zone center Γ point, i.e. $\boldsymbol{q} = (0,0,0)$. A vanishing phonon frequency results from the vanishing restoring force against the atomic displacement for the corresponding vibrational mode. Consequently, the crystal structure may undergo a displacive transition to reach a new minimal-energy configuration with lower symmetry. Our calculated ω^2 of the two most significant soft modes as a function of pressure are shown in Fig. 10. The two ω^2 are found to exhibit linear pressure dependencies. Compared with the the M-point TA mode, the softening B_u mode has a higher frequency at ambient pressure, yet it decreases much faster with the increase of pressure. Phonon frequencies of both softening modes reach zero at around 60 GPa. Although the frequency of the M-point TA phonon vanishes before the B_u branch, the predicted difference is, however, small. We thus consider both softening phonon modes as two competing mechanisms that may be responsible for the structural instability of β-Si_3N_4 at HPs. It is worth pointing out that α-Si_3N_4 does not show any signs of structural instability in our calculation, which is consistent with the observed differences in the calculated mode Grüneisen ratios [Fig. 5(a)].

The atomic displacements according to the soft M-point TA mode are in the x–y plane and the symmetry of the unit cell is reduced from hexagonal $P6_3/m$ to monoclinic $P2_1/m$ after the distortion. The magnitude of one lattice vector of the $P2_1/m$ primitive unit cell (28 atoms) is about twice that of the $\boldsymbol{a}$ vector of the original hexagonal unit cell. Constrained with the $P2_1/m$ symmetry, we calculated the minimized total energies of the distorted structure for several volumes by allowing further relaxation of both unit cell shapes and internal coordinates. The calculated E-V curve is shown in Fig. 11. According to our LDA total energy-minimization calculations, the $P2_1/m$ structure relaxes back to the original β structure at volumes larger than the 8.75 $Å^3$/atom. Yet at volumes smaller than the 8.75 $Å^3$/atom, the $P2_1/m$ phase yields a lower energy. The relaxed structure with a volume of 8.25 $Å^3$/atom is shown in Fig. 12(b). After further energy minimization, for volume 8.25 $Å^3$/atom, the lattice the parameters are $a = 13.912$ Å, $b = 6.674$ Å, and $c = 2.777$ Å. The length of a is slightly larger than twice that of b. The angle between a and b becomes 116.4° from the original 120° in β phase. The c/b ratio is getting larger compared with that in β-Si_3N_4. This is consistent

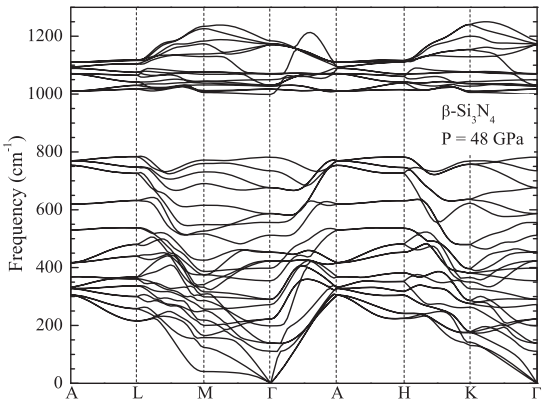

FIG. 9. Phonon dispersion of β-Si_3N_4 at a pressure of 48 GPa. Two competing soft-phonon modes are found: one TA branch at the M point and one optic branch at the Γ point. No LO-TO splitting correction is added for the interests of low-frequency modes only.

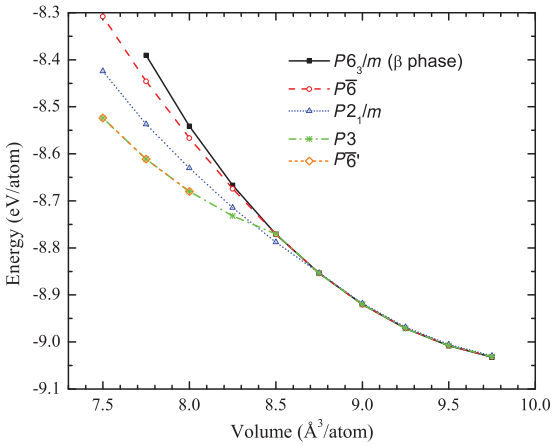

FIG. 11. (Color online) The total energy of $P6_3/m$ (β), $P\bar{6}$, $P2_1/m$, $P3$, and $P\bar{6}'$ structures as a function of volume.

with the fact that it becomes more difficult to compress along the c axis than in the x–y plane after the structural distortion. The displacements of internal coordinates can be described in terms of N atoms. Around each 2c N atom in β-Si_3N_4 there are three nearest 6h N atoms which are in the same basal plane. During the distortion, the 6h N atoms move in a way that it causes the previous planar vertical N-Si_3 units to pucker. The puckering pattern can be seen in Fig. 12(b). In the $P2_1/m$ structure, two of the nearest N atoms become closer to the "centered" 2c N atom (no longer the 2c site in the $P2_1/m$ symmetry, but it is convenient to label it consistently) but the third one moves away from it. Consequently the "centered" 2c N atom is "pushed" away by the two closer N atoms, which breaks the hexagonal symmetry and causes the three Si-N-Si bond angles to be distorted from the perfect 120°. More important, the interatomic distance between the Si atoms at the 2e site and one of their second nearest neighbors decreases rapidly upon compression. At the volume of 8.25 $Å^3$/atom, this distance is only 1.988 Å which is slightly larger than

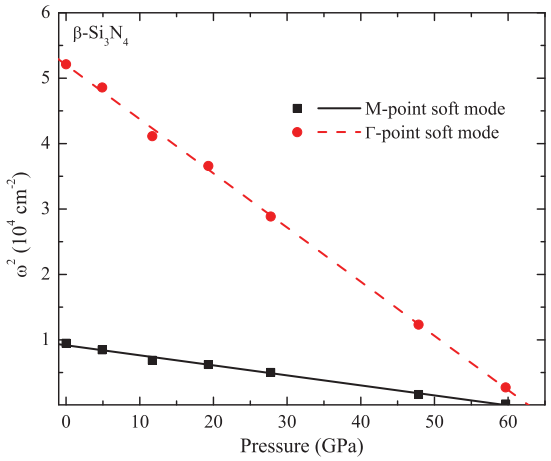

FIG. 10. (Color online) The square of vibrational frequency (ω^2) as a function of pressure for two competing soft-phonon branches: one TA branch at the M point and one B_u branch at the Γ point. Solid squares and circles represent data from calculation. Solid and dashed lines are from a linear fitting.

that of previous Si-N bonds (less than 1.7 Å). This tendency of forming an extra bond may help to stabilize the distorted structure under HPs. The new $P2_1/m$ phase is dynamically stable at pressures at least up to 75 GPa.

A similar distortion calculation was performed for the soft B_u mode at the Γ point. The atomic displacements based on the corresponding vibrational pattern yields a new structure which has a hexagonal $P\bar{6}$ symmetry. The size of the primitive unit cell is the same as β-Si_3N_4 (i.e., 14 atoms) and the displacements are still within the x–y plane. The E-V curve and data points of $P\bar{6}$ phase are shown in Fig. 11 as the (red) dashed line. Its structure returns to the β phase after fully relaxation for volumes larger than 8.75 $Å^3$/atom. Its energy is slightly lower than the β phase at a smaller volume; however, it is higher than that of the $P2_1/m$ phase. Figure 12(c) shows the relaxed $P\bar{6}$ structure at the volume of 8.25 $Å^3$/atom. The c/a ratio increases slightly compared with that of the β-Si_3N_4, and this may again be ascribed to less compressibility along the c axis. The structure of $P\bar{6}$ phase can be interpreted in terms of the puckering pattern of 6h N atoms. Unlike the $P2_1/m$ structure, as shown in Fig. 12(c), three "in-plane" 6h N atoms move clockwise and become closer to one of the "centered" 2c N atoms that has a z coordinate of 3/4 in term of c in our case. At the same time, the other three 6h N atoms move counterclockwise and become away from the other "centered" 2c N atom ($z = 1/4$).

We further calculated the phonon spectrum of the $P\bar{6}$ structure which contains 14 atoms per unit cell and discovered an optic soft-phonon mode at its Γ point. From the corresponding eigenvector, we obtained a new structure with hexagonal $P3$ symmetry. The size of its primitive unit cell is the same as that of the β phase, i.e., two formula Si_3N_4 units per cell. The E-V relation of $P3$ phase is shown in Fig. 12 as the (green) dashed dotted line. Its structure returns to the β phase beyond a volume of 8.75 $Å^3$/atom and remains stable at a smaller volume. For volumes smaller than the 8.37 $Å^3$/atom, the $P3$ phase has the lowest energy among the four structures considered here. A structure model of the $P3$ phase at the volume of 8.25 $Å^3$/atom is shown in Fig. 12(d). The c/a ratio of the $P3$ structure is very close to that of β phase.

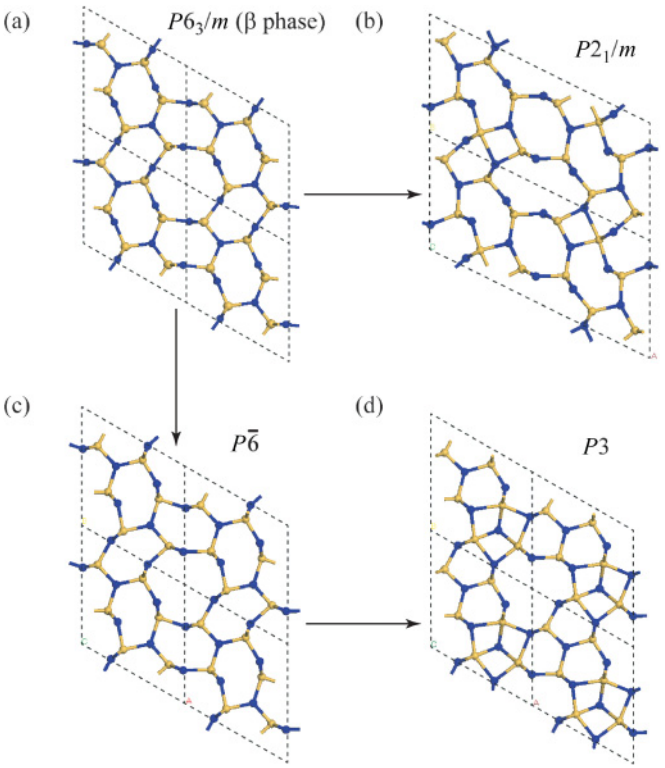

FIG. 12. (Color online) Ball-stick models of (a) $P6_3/m$, (b) $P\bar{6}$, (c) $P2_1/m$, and (d) $P3$ structures viewed along the z axis. Balls in a dark color (blue) represent N atoms, and Si atoms are in a light color (yellow).

The $P3$ structure can be understood as a further distortion of the $P\bar{6}$ phase. Relative to the $P\bar{6}$ structure, the major difference in $P3$ phase is the z coordinate of the "centered" 2c N atom which is surrounded by three closer N atoms. This "centered" 2c N atom, denoted hereafter as the puckering 2c N, is "pushed" up or down by three approaching N atoms. As the volume becomes smaller, the puckering 2c N is "pushed" by the three approaching 6h N atoms eventually to the middle of two "closer-N-atoms" layers ($z = 1/4$) and becomes six coordinated. The other "centered" 2c N atom remains its z coordinate because there is no "push" effect. For a volume between the 8.00 Å^3/atom and 8.75 Å^3/atom, which is before the puckering 2c N atom reaches its final position ($z = 1/4$), the z coordinates of other atoms deviate slightly from their previous values. However, these z coordinates recover their previous values perfectly ($z = 1/4$ and $3/4$) when the puckering 2c N atom is stabilized at $z = 1/4$. It is interesting to note that when the 2c N atoms are on the same level ($z = 1/4$), the $P3$ structure falls into the category of $P\bar{6}$ symmetry. However, this new $P\bar{6}$ phase is different from the former $P\bar{6}$ structure. To distinguish them, the latter is labeled as $P\bar{6}'$. Using the same criterion to verify the formation of bonds, there are six extra bonds being formed within a primitive unit cell, i.e., three extra bonds per formula unit. And for the $P2_1/m$ phase, it is only $1/2$ extra bonds per formula unit. To show the differences among the β, $P\bar{6}$, $P3$, and $P\bar{6}'$ structures, Wyckoff positions of these phases are listed in Table III.

D. Room-temperature metastable phase

From the E-V curves shown in Fig. 11, the transition from β-Si_3N_4 to one of the three candidates is determined by the common tangent line between them. The smallest magnitude of the slope (negative) corresponds to the lowest transition pressure, and this is made by the $P3$ phase. However, at the transition point, the structure belongs to the $P\bar{6}'$ phase. Both $P2_1/m$ and $P\bar{6}$ phases are likely bypassed. The transition pressure is estimated to be 38.5 GPa, which is comparable to the experimentally observed 35 GPa for the unidentified δ phase.[29] The transition pressure is much smaller than 60 GPa, at which one phonon frequency becomes zero in the β-Si_3N_4. It indicates that the predicted $\beta \rightarrow P\bar{6}'$ transition is of first order, and the predicted volume reduction is about 10.8%.

To estimate the kinetic barrier height in the $\beta \rightarrow P\bar{6}'$ transition, we calculated the enthalpy landscape in terms of the atomic displacements in the x–y plane and the z coordinate of the puckering 2c N atom. At the transition pressure, we took the β phase as the starting structure and the $P\bar{6}'$ phase as the ending structure. Two transition parameters, i.e., f_{x-y} and f_z, were used to linearly interpret the phase transition. Initial internal coordinates of the intermediate structure can be expressed as

$$\begin{aligned} x &= x_i + (x_f - x_i) f_{x-y}, \\ y &= y_i + (y_f - y_i) f_{x-y}, \\ z &= z_i + (z_f - z_i) f_z, \end{aligned} \tag{8}$$

TABLE III. Atomic coordinates (Wyckoff positions) of the β, $P\bar{6}$, $P3$, and $P\bar{6}'$ structures at specified volumes. For comparison, the Wyckoff sites are grouped according to the β phase.

	β	$P\bar{6}$	$P3$	$P\bar{6}'$
Space group	$P6_3/m$	$P\bar{6}$	$P3$	$P\bar{6}$
Z	2	2	2	2
Volume (Å^3/atom)	8	8	8.25	8
N1	2*c* (1/3,2/3,1/4)	1*c* (1/3,2/3,0)	1*b* (1/3,2/3,0.300)	1*c* (1/3,2/3,0)
		1*f* (2/3,1/3,1/2)	1*c* (2/3,1/3,0.333)	1*e* (2/3,1/3,0)
N2	6*h* (0.324,0.013,1/4)	3*j*/ (0.269,0.013,0)	3*d* (0.270,0.003,0.277)	3*j*/ (0.261,0.005,0)
		3*k* (0.630,0.994,1/2)	3*d* (0.625,0.021,0.795)	3*k* (0.623,0.021,1/2)
Si	6*h* (0.155,0.748,1/4)	3*j*/ (0.148,0.741,0)	3*d* (0.136,0.733,0.293)	3*j*/ (0.136,0.734,0)
		3*k* (0.853,0.257,1/2)	3*d* (0.860,0.294,0.773)	3*k* (0.860,0.293,1/2)

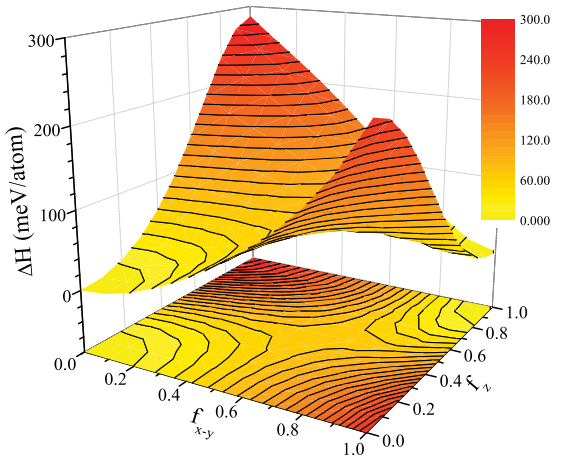

FIG. 13. (Color online) Enthalpy landscape and its contour plot as a function of f_{x-y} and f_z at the transition pressure of 38.5 GPa.

where the subscripts i and f denote the starting (initial) and ending (final) structures, respectively. Both f_{x-y} and f_z range from 0 to 1, and they can be set independently. 10×10 uniform grids were adopted for the intermediate structures. In the total energy calculation of each structure, by fixing the internal coordinates, we allowed the external parameters to relax. Because this transition is observed to occur at RT, it is a good approximation to use enthalpy instead of Gibbs free energy to investigate the phase transition. The enthalpy landscape and its contour plot as functions of f_{x-y} and f_z at 38.5 GPa are shown in Fig. 13. Two minimum points correspond to the β (0,0) and $P\bar{6}'$ (1,1) structures. The transition path is given by the gradient curve connecting the two minimum points. It passes the saddle point which provides the transition barrier height. The pathway we predict is close to the linear path that f_{x-y} and f_z vary at similar paces. The calculated saddle point is located at (0.6,0.5) and the corresponding enthalpy barrier is 67.23 meV/atom. To overcome this barrier, certain activation temperature is necessary to stimulate the atomic vibrations to a level that is comparable to ΔH. Using the Dulong and Petit law $E = 3k_BT$, the "threshold" activation temperature is estimated to be 260 K, which is lower than the RT. Since all the internal coordinates were fixed in our calculation, the activation temperature should be considered as an upper limit to its actual value. The $\beta \rightarrow P\bar{6}'$ transformation should be interpreted as a low-barrier transition induced by softening phonon modes. The method adopted here for calculating the kinetic enthalpy barrier has been successfully applied to the Corundum $\rightarrow$ Rh_2O_3(II) transition in Al_2O_3 previously.[69]

It is interesting to point out that the new $P\bar{6}'$ phase is dynamically stable above the transition pressure (i.e., 38.5 GPa). However, one of its TA branches shows a tendency to vanish at the K point below the transition pressure. The atomic displacements according to the K-point softening mode suggest a structure which belongs to $P3$ symmetry, but the unit cell is three times larger than the previous $P3$ phase, i.e., six formula units per primitive unit cell. To distinguish this from the previous $P3$-Si_3N_4, we will denote this second $P3$ structure as the $P3'$ phase later on. Taking the $P3'$ structure as the initial structure, we performed total energy calculations with both internal and external parameters being fully relaxed. $P3'$ phase is found to exist only between the volume of the 8 Å^3/atom and the 8.75 Å^3/atom. Its structure relaxes back to the β structure for volumes larger than the 8.75 Å^3/atom and becomes $P\bar{6}'$ phase for volumes smaller than the 8 Å^3/atom. Its energy is slightly lower than that of the $P3$ phase by merely a few meV/atom. The structure of the $P3'$ phase is very similar to that of the $P3$ phase except the z coordinates of each $P3$ Wyckoff site split into three different values with small deviations. In another words, the $P3$ phase is a special case of the $P3'$ structure. As indicated in the calculated enthalpy landscape shown in Fig. 13, the transition path is close to the linear path along which f_{x-y} and f_z vary cooperatively. We take the $P3'$ phase as, an intermediate state connecting β and $P\bar{6}'$ structures; the enthalpy barriers at 30 and 38.5 GPa are shown in Fig. 14, together with the barriers from direct $\beta \rightarrow P\bar{6}'$ transition as a comparison. The barrier heights along these two paths are very comparable. The ΔH in $\beta \rightarrow P3' \rightarrow P\bar{6}'$ path is lower than the $\beta \rightarrow P\bar{6}'$ path by only 5.6 meV/atom at 38.5 GPa and 9.8 meV/atom at 30 GPa.

Our predicted $P\bar{6}'$ phase has a hexagonal symmetry which is different from what Zerr proposed based on the EDXD pattern.[29] However, the interplanar spacings for the six peaks he observed could also be assigned to a crystal system with hexagonal symmetry. Supportive evidence is that Soignard *et al.*[31] observed a similar $\beta \rightarrow P3$ metastable transition in Ge_3N_4. They claimed that Zerr's δ-Si_3N_4 is likely to be analogous to their observed δ-Ge_3N_4 based on comparison of the x-ray diffraction and Raman data. Next, we will examine the structure of δ-Si_3N_4 from a HP experiment.

E. High-pressure experiment

Our RT compression studies of β-Si_3N_4 using synchrotron angle-dispersive x-ray diffraction (ADXRD) techniques and Raman scattering confirmed the results of Zerr that a phase transition into a δ-Si_3N_4 polymorph occurs at $P = 35-36$ GPa that is reversible upon decompression.[29] However, the x-ray diffraction peaks of the HP δ-Si_3N_4 phase do not

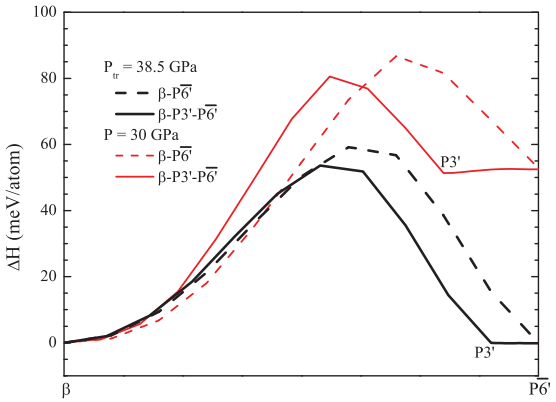

FIG. 14. (Color online) Enthalpy barrier (relative to the β phase) as a function of linearly interpreted transition parameter at 30 GPa (red, gray) and the transition pressure of 38.5 GPa (black). The solid curves denote the $\beta \rightarrow P3' \rightarrow P\bar{6}'$ path, and the dashed curves denote direct $\beta \rightarrow P\bar{6}'$ path. The horizontal axis is defined as qualitative structural similarity. The left end represents the β structure, and the right end represents the $P\bar{6}'$ structure.

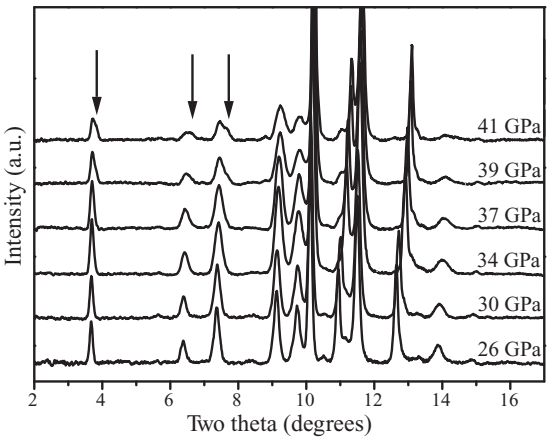

FIG. 15. x-ray diffraction patterns of the compression of the β-Si_3N_4 phase from 26 GPa and the formation of the δ-Si_3N_4 phase emerging at 37 GPa and continuing to 41 GPa. The arrows highlight the positions of the peaks associated with the formation of the δ phase. The wavelength used in the monochromatic synchrotron x-ray diffraction was $\lambda = 0.444$ Å

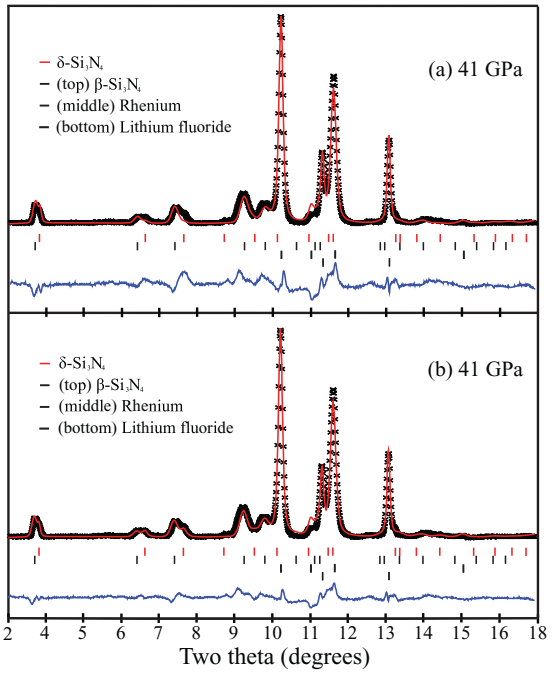

FIG. 16. (Color online) Rietveld refinements of diffraction data obtained of both the δ and β phases of Si_3N_4 in a lithium fluoride pressure-transmitting medium at 41 GPa. Data points and Rietveld fit are overlaid in black and red (gray), respectively, the difference plot is shown. The red (gray) tick marks indicate peaks for δ-Si_3N_4, the top black tick marks indicate peaks for β-Si_3N_4, and the middle black tick marks are of the Rhenium gasket, and the bottom black ones are of the LiF pressure medium. (a) Data obtained at 41 GPa of both the δ and β phases of Si_3N_4. The internal atomic coordinates used for the refinement are fixed according to the values generated from the DFT calculations. (b) The same data set as (a) at 41 GPa but with the atomic coordinates refined. The wavelength used in the monochromatic synchrotron x-ray diffraction was $\lambda = 0.444$ Å

correspond to those of predicted "postspinel" polymorphs, including the wII structure. Instead the x-ray patterns closely resemble those of the starting β-Si_3N_4 material, and they can be readily indexed to a $P3$ or $P\bar{6}$ structure as predicted theoretically (Figs. 12, 15, 16). The behavior is similar to that reported for β-Ge_3N_4 in which a sequence of two soft mode transitions or a first-order transformation occurs between the β and δ phases during compression, resulting in a variation of the starting phenacite structure.[32] That interpretation is consistent with the results of the present theoretical study. The x-ray diffraction results provide evidence that the β and δ polymorphs coexist over a pressure range providing support for a first-order nature of the phase transition (Fig. 15). The volume reduction at the transition pressure is about 9.25%, which is close to the theoretically predicted value (10.8%).

This coexistence between the two phases and the diffraction features of the δ structure only emerging as shoulders on β structure peaks demanded a comparative Rietveld refinement approach. As no defining feature owing to the δ structure is isolated and easy to refine as a stand-alone peak, the refinement procedure was carefully undertaken. Figure 16 shows two different refinements of the same diffraction data but using in (a) just the fixed atomic coordinates as generated by the DFT calculations for describing the δ-Si_3N_4. This produced wRp and Rp values of 0.1420 and 0.1025, respectively. In (b) the general atomic coordinates were hand picked but were then permitted to refine. This gave rise to wRp and Rp values of 0.1263 and 0.0895 respectively. The approach in (a) allowed us to validate the consistency of the theoretical model to the experimental results observed. Importantly, although the model with the refined atomic coordinates of the δ phase in (b) produced a better fit, the fact that the refinement package was trying to fit only undefined diffraction features does not produce a convincing enough case to publish the refined positions but in fact strengthens the importance of the reliance on theory for when looking at powder diffraction data from high-energy sources at elevated pressures.

Raman spectra obtained during compression of the β-Si_3N_4 phase in a 4:1 methanol-ethanol medium to 43 GPa followed by subsequent decompression are shown in Fig. 17(a). Up to 30 GPa, the observed pressure shifts closely match those predicted in the theoretical study (Fig. 8). Above 34 GPa a new set of peaks is observed to appear in the spectrum, indicating the onset of the transition into the δ-Si_3N_4 phase (Figs. 17, 18). The low-frequency peaks match closely those described by Zerr in his first study documenting the occurrence of δ-Si_3N_4.[29] On decompression, the characteristic spectrum of the β-Si_3N_4 phase is recovered below 30–33 GPa, indicating some hysteresis and likely coexistence of the β and δ forms already noted from the analysis of the synchrotron x-ray diffraction results. The behavior in the high-frequency region is unusual, in that a broad band appears in the range expected for Si-N stretching vibrations (900-1150 cm^{-1}) at above 34–36 GPa, which disappears upon decompression. No such broad feature was shown in the data presented by Zerr,[29] during Raman spectroscopy carried out within an Ar pressure-transmitting medium (PTM). It is possible that this broad band might arise from the methanol-ethanol mixture that has become an amorphous solid at these HPs, but that does not appear to be the case in recent studies of B_4C compressed in

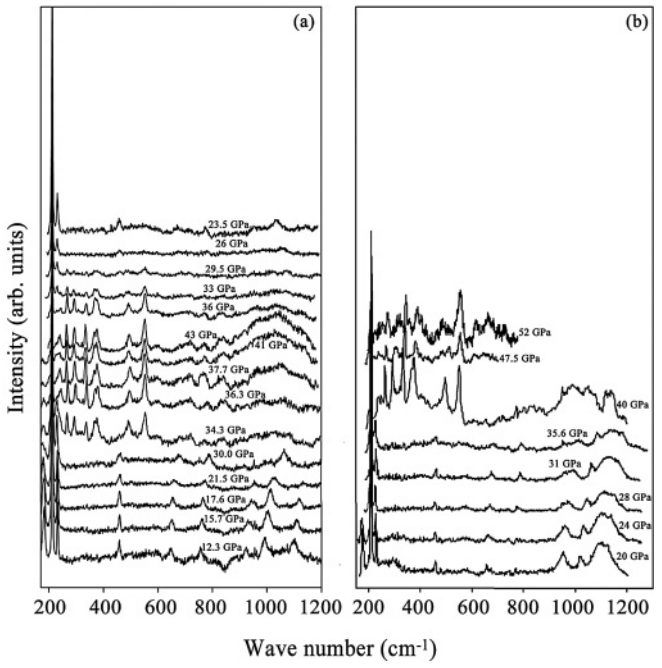

FIG. 17. Raman spectra of (a) the compression and decompression of the β-Si_3N_4 phase up to 43 GPa, using 4:1 methanol-ethanol as the PTM. (b) The compression of the β-Si_3N_4 phase up to 52 GPa, using N_2 as the PTM.

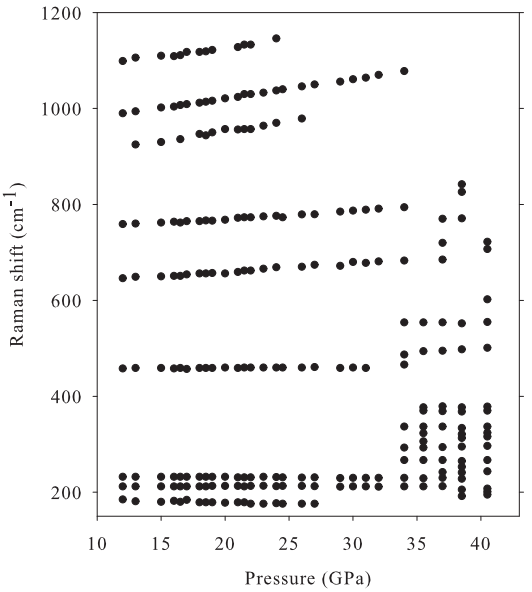

FIG. 18. Pressure dependencies of the observed Raman peaks for compression of the β-Si_3N_4 up to 43 GPa. Additional Raman peaks above ~34 GPa are associated with the formation of the δ phase.

the medium to the same pressure range.[70] Another possibility is that the broadened high-frequency peaks might appear due to the nonhydrostatic nature of the PTM. We also obtained data using N_2 as a PTM [Fig. 17(b)]. In this case the high-frequency modes resemble more closely those reported by Zerr,[29] but there is still a significantly broadened feature in the 900–1150 cm^{-1} range.

The appearance of this broad feature, occurring throughout the range expected for Si-N stretching vibrations, might be due to some disordering mechanism occurring within the Si_3N_4 sample, experienced as it undergoes its "$\beta \rightarrow \delta$" transition. Theoretically, a metastable phase with $P3$ symmetry ($P3'$ phase) was found to be competitive with the $P\bar{6}'$ structure in the vicinity of the pressure-induced transition from the β-Si_3N_4 structure. Competition between the two potential structure solutions could result in disorder in the N sites and perhaps also Si positions, resulting in broadening of the high-frequency vibrational bands. Any deviations from a hydrostatic compression environment could significantly affect such slight, modifications to sampling the stable vs. metastable structures predicted to be present, and we believe that this is the case here. Interestingly, however, the methanol-ethanol pressure medium used in our first study is expected to remain a hydrostatic fluid until ~10 GPa, whereas N_2 and Ar undergo solidification transitions that result in nonhydrostatic behavior above the 2–3 GPa range.[71,72]

F. Thermal properties

Using our first-principles-calculated thermodynamic potentials, we further derived thermal properties of Si_3N_4 over a wide T-P range. Since currently the experimental thermal properties data are available for only β- and γ-Si_3N_4, we mainly focus on discussion of these two phases.

Figure 19 shows the volume TECs of β-Si_3N_4 as a function of temperature at zero pressure. The experimental data (measured at ambient pressure) are widely scattered in both low T and high T regions which may be attributed to the differences in samples and experimental techniques. Above RT, our predicted TEC is closer to the measured data of Schneider (except a couple of scattered data points above 1200 K), which is the lower bound of all the reported experimental data. Compared with the calculation of Kuwabara *et al.*,[22] our predicted TEC are slightly lower. Nevertheless, the difference is noticeable at both low and high temperatures. At present, there is only one experimental report on the TECs at low temperatures.[37] However, the measured data are significantly higher than both calculations at low temperatures. And, more important, no trend of negative TEC is revealed near 0 K, which is questionable. A negative TEC at low T is predicted by both calculations, and is related to the instability of β phase under pressure, as discussed later in the paper. The difference between the two calculations at high temperatures can be partially attributed to the fact that static energies are fitted to the second-order and third-order BM-EOS, respectively, in Kuwabara's and our calculations (in both calculations, the thermal free energies are fitted to the second-order BM-EOS). The second-order BM-EOS model assumes that the pressure derivative of the bulk modulus is fixed to 4. Adopting the same type of second-order BM-EOS for the static energies, we find that our calculated TECs (not shown in the figure) increase moderately at high temperatures, about half way between the two calculated TECs shown in the figure. At the same time, the order of BM-EOS, for the static energies does not affect the prediction below RT. Therefore, the discrepancy between the two theoretical TEC curves likely also originates from the differences in the calculated phonon density of states.

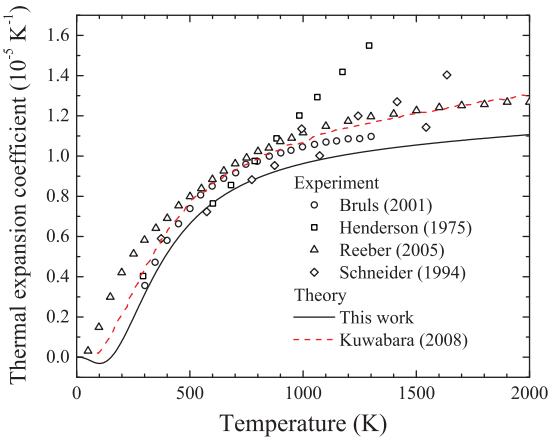

FIG. 19. (Color online) Temperature dependence of volume TEC of bulk β-Si_3N_4 at zero pressure. Solid line denotes present work, dashed line (red) denotes the first-principles calculation from Kuwabara *et al.*,[22] and discrete symbols denote experimental data.[34–37]

Another thermal property that is closely related to the TEC (α) is the bulk Grüneisen parameter (γ): $\alpha = \gamma C_V/(B_T V)$, where C_V, B_T, and V are heat capacity, bulk modulus, and volume, respectively. Figure 20 shows our calculated Grüneisen parameter of β-Si_3N_4, together with reported experimental data.[36] Our calculated bulk Grüneisen parameter is in excellent agreement with Bruls' measurement. The estimated percentage difference between experiment and calculation is within 10% for 300 K $< T <$ 500 K, and the difference is gradually reduced to about 2% at $T =$ 1300 K. The excellent theory-experiment agreement in the temperature range between 300 and 1300 K validates our calculation and supports our theoretical prediction that the bulk Grüneisen parameter (γ) turns negative below 200 K in β-Si_3N_4. Since C_V, B_T, and V are all positively defined, TEC (α) always has the same sign as the bulk Grüneisen parameter (γ). Within the QHA, γ is the weighted average of mode Grüneisen ratios [Eq. (4)]. At low temperaturs, only low-frequency phonons are thermally excited and contribute to the bulk Grüneisen ratios. In the case of α and β phases, many low-frequency phonons have negative mode Grüneisen ratios (Fig. 5). This yields the

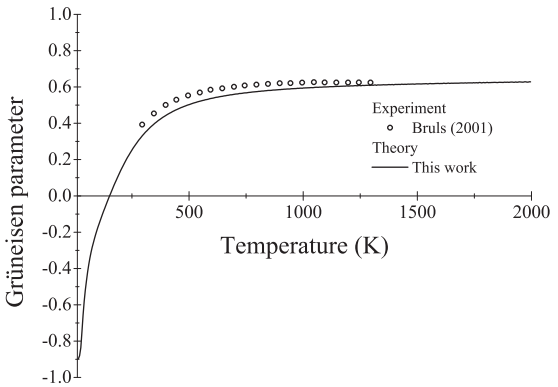

FIG. 20. Temperature dependence of bulk Grüneisen parameter of β-Si_3N_4 at zero pressure. Solid line denotes present work, and discrete symbols denote experimental data.[36]

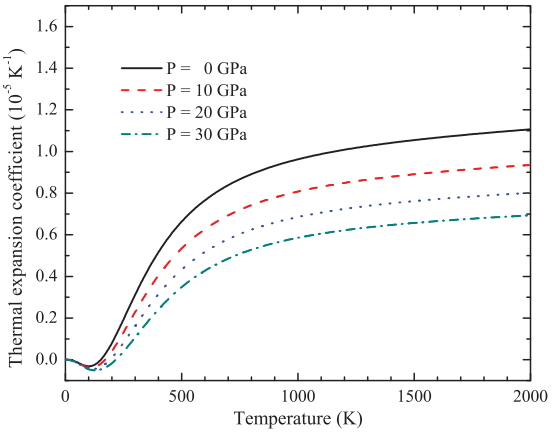

FIG. 21. (Color online) Temperature dependence of volume TEC of bulk β-Si_3N_4 at pressures of 0, 10, 20, and 30 GPa.

negative overall bulk Grüneisen parameters, and consequently leads to the negative TEC at low temperatures. For the β phase, the two branches that correspond to the most negative mode Grüneisen parameters are found to be the softening M-point TA and Γ-point B_u modes, which are responsible for the instability of β-Si_3N_4 at HPs.

We also examined the pressure effects on TEC of β-Si_3N_4. As pressure increases from 0 to 30 GPa, our calculated TEC decreases from 1.11×10^{-5} to 0.69×10^{-5} K^{-1} at 2000 K (Fig. 21). At the same time, the negative TEC range extends from below 150 K at 0 GPa to 220 K at 30 GPa. The magnitude of the negative TEC value also increases from -3.11×10^{-7} to -5.09×10^{-7} K^{-1}. This pressure effect of TEC in β-Si_3N_4 is in agreement with the calculated pressure effect on low-frequency phonon modes and the soft-phonon-associated structural instability discussed in earlier sections.

Figure 22 shows the experimental and calculated TEC of γ-Si_3N_4 at ambient pressure.[22,40–42] As a contrast, we also plot the calculated TEC of the two hexagonal phases of Si_3N_4. Although the cubic γ phase is nearly 20% denser and more than 20% less compressible than the two hexagonal phases, its TEC is more than twice as large as those of the hexagonal phases, indicating that there is a significantly stronger lattice anharmonicity in the cubic γ phase. This may also be related

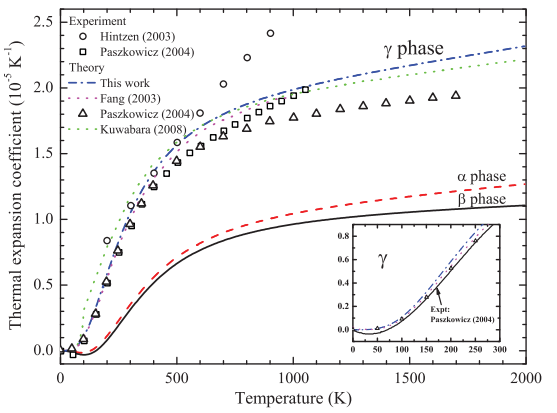

FIG. 22. (Color online) Temperature dependencies of volume TECs of α-, β-, and γ-Si_3N_4 at zero pressure. The inset shows the low-temperature TEC of the γ phase from 0 to 300 K.

to the fact that the Si-N bond lengths in the γ phase are larger than those in the α and β phases.

The TECs of γ-Si_3N_4 remains significantly larger than those hexagonal phases over the wide T-P ranges in our calculations. For example, at 30 GPa, the TECs of the most stable γ phase is still about twice as large as that of the β phase. It is also interesting to mention that, although our calculation predicts that the ground state β phase has lower TECs than the meta-stable α phase at zero pressure, the order of the TECs in the two hexagonal phases switches upon compression, At 30 GPa, the α phase is predicted to have the lowest TECs.

The two sets of experimental TECs of γ-Si_3N_4 are relatively close below 500 K, but they differ significantly at higher temperatures, which may originate from the differences in samples and measurement methods. Overall, our calculation is in better agreement with the experimental data of Paszkowicz *et al.*,[41] and the theoretical data of Fang *et al.*[42] The calculation reported by Paszkowicz *et al.*, which is based on a simplified Debye model to approximate the phonon density of states,[41] is consistent with our data at temperatures below 500 K. However, their predicted TECs at high temperatures is apparently lower than all other three calculations that are based on the first-principles phonon density of states. At low temperatures, the prediction of γ-Si_3N_4 from the Kuwabara *et al.* is noticeably larger than other calculations, including ours. The same type of overestimation also occurs for the low-T TEC of the β phase (Fig. 19).

As illustrated in the inset of Fig. 22, Paszkowicz *et al.* reported that the measured TEC of γ-Si_3N_4 drops below zero for $T < \sim 70$ K.[41] However, this is in disagreement with all the reported calculations. From the discussion in the above text, the TEC at low temperatures is affected by the mode Grüneisen ratios of the low-frequency phonon modes. As shown in Fig. 5(c), no negative mode Grüneisen ratios are found in the γ-Si_3N_4. The bulk Grüneisen parameter of γ-Si_3N_4 must be positive at all temperatures, and consequently, TEC of γ-Si_3N_4 must be positive at all temperatures.

IV. CONCLUSION

In this paper, first, we have theoretically studied the equilibrium thermodynamic stability and high-pressure phase transitions among the α-, β- and γ-Si_3N_4 within the frame of density functional theory (DFT) and quasi harmonic approximation (QHA). We find that α-Si_3N_4 remains as a metastable phase at temperatures up to 2000 K and pressures up to 10 GPa. The equilibrium $\beta \rightarrow \gamma$ transition pressure is predicted as 7.5 GPa at 300K and it increases to 9.0 GPa at 2000 K, and the $\alpha \rightarrow \gamma$ transition pressure is about 0.5 GPa lower than that of the $\beta \rightarrow \gamma$ transition.

Next we have combined first-principles calculation and high-pressure experiments (x-ray diffraction and Raman) to understand the pressure-induced $\beta \rightarrow \delta$ transition at RT. From our calculated phonon dispersion, both α- and β-Si_3N_4 are dynamically stable at low pressurs. However, two competing phonon-softening mechanisms are found in the β phase at HPs. β-Si_3N_4 is predicted to undergo a first-order $\beta \rightarrow P\bar{6}'$ transition above 38.5 GPa, while α-Si_3N_4 shows no signs of dynamical instability. The predicted metastable high-pressure $P\bar{6}'$ phase is structurally related to the β-Si_3N_4. The enthalpy barrier height is estimated as only 67.23 meV/atom. The predicted results are consistent with the observed $\beta \rightarrow \delta$ transition at RT. Our experimental x-ray diffraction and Raman scattering measurements confirm the transition at about 34 GPa, and support the postphenacite nature of the structure of the δ phase. The $\beta \rightarrow \delta$ transition in Si_3N_4 is analogous to the $\beta \rightarrow \delta$ transition in Ge_3N_4. The possibility for the δ phase to adopt the postspinel structure has been excluded.

Furthermore, we have clearly demonstrated that softening of phonon modes upon compression also affects the thermal properties at low temperatures. We have shown that the low-frequency phonon modes that have negative mode Grüneisen ratios lead to negative calculated TEC in both α- and β-Si_3N_4, and we have predicted that no negative TEC exists in γ-Si_3N_4. Our predicted thermal properties, including TEC and bulk Grüneisen parameters, are in good agreement with available experimental data at ambient pressure.

ACKNOWLEDGMENTS

We acknowledge the support from the Department of Energy (Grant Nos. DE-FG02-03ER46060) and National Science Foundation (Grant Nos. HRD-0317741 and EAR-0757847). Experimental work by PFM, OS and AS were supported by UK EPSRC Grant Nos. EP/D504782 and EP/D07357X (Senior Research Fellowship) to PFM. We also thank Dominik Daisenberger and Edward Bailey for their assistance with experimental measurements.

*Author to whom correspondence should be addressed : bbixu@physics.auburn.edu

[1] K. Komeya and M. Matsui, *Materials Science and Technology*, edited by R. W. Cahn, P. Haasen, and E. J. Kramer (Wiley-VCH, Weinheim, 1994), Vol. 11, pp. 518–565.

[2] F. Schröder, *Gmelin Handbook of Inorganic and Organometallic Chemistry*, Vol. Si Suppl. B 5c of Silicon Nitride in Electronics, series (Springer-Verlag, Berlin, 1991).

[3] A. Zerr, G. Miehe, G. Serghiou, M. Schwarz, E. Kroke, R. Riedel, H. Fueß, P. Kroll, and R. Boehler, Nature (London) **400**, 340 (1999).

[4] M. Schwarz, G. Miehe, A. Zerr, E. Kroke, B. T. Poe, H. Fuess, and R. Riedel, Adv. Mater. **12**, 883 (2000).

[5] T. Sekine, H. He, T. Kobayashi, M. Zhang, and F. Xu, Appl. Phys. Lett. **76**, 3706 (2000).

[6] E. Soignard, M. Somayazulu, J. J. Dong, O. F. Sankey, and P. F. McMillan, J. Phys. Condens. Matter **13**, 557 (2001).

[7] Y. Zhang, A. Navrotsky, and T. Sekine, J. Mar. Res. **21**, 41 (2006).

[8] R. Grün, Acta Crystallogr. Sec. B **567**, 7408 (1979).

[9] F. Gao, W. Yang, Y. Fan, and L. An, Nanotechnology. **19**, 105602 (2008).

[10] J. Liang, L. Topor, A. Navrotsky, and M. Mitomo, J. Mater. Res. **14**, 1959 (1999).

[11] C. Greskovich and S. Prochazka, J. Am. Ceram. Soc. **60**, 471 (1977).

[12]L. J. Bowen, R. J. Weston, T. G. Carruthers, and R. J. Brook, J. Mater. Sci. **13**, 341 (1978).
[13]M. Shimada, N. Ogawa, M. Koizumi, F. Dachille, and R. Roy, Am. Ceram. Soc. Bull. **58**, 519 (1979).
[14]L. J. Gauckler, H. Hohnke, and T. Y. Tien, J. Am. Ceram. Soc. **63**, 35 (1980).
[15]K. H. Jack, *Progress in Nitrogen Ceramics*, edited by R. F. L. (Martinus Nijhoff, Boston, 1983), pp. 45–60.
[16]J. Y. Park, J. R. Kim, and C. H. Kim, J. Am. Ceram. Soc. **70**, 240 (1987).
[17]H. Hirai and K. Kondo, J. Am. Ceram. Soc. **77**, 487 (1994).
[18]H. Suematsu, M. Mitomo, T. E. Mitchell, J. J. Petrovic, O. Fukunaga, and N. Ohashi, J. Am. Ceram. Soc. **80**, 615 (1997).
[19]H. Suematsu, J. J. Petrovic, and T. E. Mitchell, Mater. Res. Soc. Symp. Proc. **287**, 449 (1992).
[20]W. Y. Ching, L. Ouyang, and J. D. Gale, Phys. Rev. B **61**, 8696 (2000).
[21]J. A. Wendel and W. A. Goddard, J. Chem. Phys. **97**, 5048 (1992).
[22]A. Kuwabara, K. Matsunaga, and I. Tanaka, Phys. Rev. B **78**, 064104 (2008).
[23]J. Z. Jiang, F. Kragh, D. J. Frost, K. Stahl, and H. Lindelov, J. Phys. Condens. Matter **13**, 515 (2001).
[24]T. Sekine and T. Mitsuhashi, Appl. Phys. Lett. **79**, 2719 (2001).
[25]P. Kroll, J. Solid State Chem. **176**, 530 (2003).
[26]A. Togo and P. Kroll, J. Comput. Chem. **29**, 2255 (2008).
[27]P. Kroll and J. Von Appen, Phys. Status Solidi B **226**, R6 (2001).
[28]K. Tatsumi, I. Tanaka, H. Adachi, F. Oba, and T. Sekine, J. Am. Ceram. Soc. **85**, 7 (2002).
[29]A. Zerr, Phys. Status Solidi B **227**, R4 (2001).
[30]P. McMillan, O. Shebanova, D. Daisenberger, R. Cabrera, E. Bailey, A. Hector, V. Lees, D. Machon, A. Sella, and M. Wilson, Phase Transitions **10**, 1003 (2007).
[31]E. Soignard, P. McMillan, C. Hejny, and K. Leinenweber, J. Solid State Chem. **177**, 299 (2004).
[32]J. Dong, O. F. Sankey, S. K. Deb, G. Wolf, and P. F. McMillan, Phys. Rev. B **61**, 11979 (2000).
[33]P. F. McMillan, S. K. Deb, and J. J. Dong, J. Raman Spectrosc. **34**, 567 (2003).
[34]C. M. B. Henderson and D. Taylor, Trans. J. Brit. Ceramic Soc. **74**, 49 (1975).
[35]J. Schneider, F. Frey, N. Johnson, and K. Laschke, Z. Kristallogr. **209**, 328 (1994).
[36]R. J. Bruls, H. T. Hintzen, G. de With, R. Metselaar, and J. C. van Miltenburg, J. Phys. Chem. Solids **62**, 783 (2001).
[37]R. R. Reeber, Therm. Conduct. **27**, 525 (2005).
[38]M. Kuriyama, Am. Ceram. Soc. Bull. **57**, 1119 (1978).
[39]V. I. Koshchenko and G. Ya, Inorg. Mater. **18**, 903 (1982).
[40]H. T. Hintzen, M. R. M. M. Hendrix, H. Wondergem, C. M. Fang, T. Sekine, and G. de With, J. Alloys Compd. **351**, 40 (2003).
[41]W. Paszkowicz, R. Minikayev, P. Piszora, M. Knapp, C. Bahtz, J. M. Recio, M. Marques, P. Mori-Sanchez, L. Gerward, and J. Z. Jiang, Phys. Rev. B **69**, 52103 (2004).
[42]C. M. Fang, G. A. de Wijs, and H. T. Hintzen, J. Appl. Phys. **93**, 5175 (2003).
[43]L. G. Wang, J. X. Sun, W. Yang, and R. G. Tian, Acta Phys. Pol. A **114**, 807 (2008).
[44]D. Vanderbilt, Phys. Rev. B **41**, 7892 (1990).
[45]G. Kresse and J. Furthmüller, Phys. Rev. B **54**, 11169 (1996).
[46]F. Birch, J. Appl. Phys. **9**, 279 (1938).
[47]F. Birch, Phys. Rev. **71**, 809 (1947).
[48]K. Kunc and R. M. Martin, Phys. Rev. Lett. **48**, 406 (1982).
[49]X. Tang, J. Dong, P. Hutchins, O. Shebanova, J. Gryko, P. Barnes, J. K. Cockroft, M. Vickers, and P. F. McMillan, Phys. Rev. B **74**, 014109 (2006).
[50]H. K. Mao, P. M. Bell, J. W. Shaner, and D. J. Steinberg, J. Appl. Phys **49**, 3276 (1978).
[51]E. Soignard and P. F. McMillan, Chem. Mater. **16**, 3533 (2004).
[52]G. N. Greaves, C. R. A. Catlow, G. E. Derbyshire, M. I. McMahon, R. J. Nelmes, and G. van der Laan, Nat. Mater. **7**, 827 (2008).
[53]A. Hammersley, S. Svensson, M. Hanfland, A. Fitch, and D. Hausermann, High Press. Res. **14**, 235 (1996).
[54]A. C. Larson and R. B. Von Dreele, Los Alamos National Lab. Rep. LAUR, 86 (2000).
[55]B. H. Toby, J. Appl. Crystallogr. **34**, 210 (2001).
[56]S. Ogata, N. Hirosaki, C. Kocer, and Y. Shibutani, Acta Mater. **52**, 233 (2004).
[57]M. Yashima, Y. Ando, and Y. Tabira, J. Phys. Chem. B **111**, 3609 (2007).
[58]H. Toraya, J. Appl. Crystallogr. **33**, 95 (2000).
[59]M. B. Kruger, J. H. Nguyen, Y. M. Li, W. A. Caldwell, M. H. Manghnani, and R. Jeanloz, Phys. Rev. B **55**, 3456 (1997).
[60]R. F. Zhang, S. H. Sheng, and S. Veprek, Appl. Phys. Lett. **90**, 191903 (2007).
[61]D. du Boulay, N. Ishizawa, T. Atake, V. Streltsov, K. Furuya, and F. Munakata, Acta Crystallogr. Sect. B: Struct. Sci. **60**, 388 (2004).
[62]Y. M. Li, M. B. Kruger, J. H. Nguyen, W. A. Caldwell, and R. Jeanloz, Solid State Commun. **103**, 107 (1997).
[63]H. He, T. Sekine, T. Kobayashi, H. Hirosaki, and I. Suzuki, Phys. Rev. B **62**, 11412 (2000).
[64]A. Zerr, M. Kempf, M. Schwarz, E. Kroke, M. Goken, and R. Riedel, J. Am. Ceram. Soc. **85**, 86 (2002).
[65]J. W. Swegle, J. Appl. Phys. **68**, 1563 (1990).
[66]R. Rao, A. M. Rao, B. Xu, J. J. Dong, S. Sharma, and M. K. Sunkara, J. Appl. Phys. **98**, 094312 (2005).
[67]E. Soignard, D. Machon, P. F. McMillan, J. J. Dong, B. Xu, and K. Leinenweber, Chem. Mater. **17**, 5465 (2005).
[68]A. Zerr, G. Miehe, G. Serghiou, M. Schwarz, E. Kroke, R. Riedel, and R. Boehler, in: Sci. and Technol. of High Press., Eds. M. H. Manghnani, W. J. Nellis and M. F. Nicol, University Press, Hyderabad 2000 (p. 914)
[69]B. Xu, H. Stokes, and J. J. Dong, J. Phys. Condens. Matter **22**, 315403 (2010).
[70]J. Guo, L. Zhang, T. Fujita, T. Goto, and M. Chen, Phys. Rev. B **81**, 060102 (2010).
[71]R. J. Angel, M. Bujak, J. Zhao, G. D. Gatta, and S. D. Jacobsen, J. Appl. Crystallogr. **40**, 26 (2007).
[72]S. Klotz, J. Chervin, P. Munsch, and G. Marchand, J. Phys. D: Appl. Phys. **42**, 075413 (2009).